1368 *Inorg. Chem.* **2011**, *50*, 1368–1377
DOI: 10.1021/ic101943h

Inorganic Chemistry
Article

Xanthene-Modified and Hangman Iron Corroles

Matthias Schwalbe,[†,§] Dilek K. Dogutan,[†] Sebastian A. Stoian,[†,‡] Thomas S. Teets,[†] and Daniel G. Nocera*[,†]

[†]*Department of Chemistry, Massachusetts Institute of Technology, 77 Massachusetts Avenue, Cambridge, Massachusetts 02139, United States, and* [‡]*Department of Chemistry, Carnegie Mellon University, 4400 Fifth Avenue, Pittsburgh, Pennsylvania 15213, United States.* [§]*Current address: Department of Chemistry, Humboldt Universität zu Berlin, Brook-Taylor-Strasse 2, 12489, Berlin; E-mail: matthias.schwalbe@chemie.hu-berlin.de*

Received September 25, 2010

Iron corroles modified with a xanthene scaffold are delivered from easily available starting materials in abbreviated reaction times. These new iron corroles have been spectroscopically examined with particular emphasis on defining the oxidation state of the metal center. Investigation of their electronic structure using ^{57}Fe Mössbauer spectroscopy in conjunction with density functional theory (DFT) calculations reveals the non-innocence of the corrole ligand. Although these iron corroles contain a formal Fe(IV) center, the deprotonated corrole macrocycle ligand is one electron oxidized. The electronic ground state of these complexes is best described as an intermediate spin $S = {}^3/_2$ Fe(III) site strongly antiferromagnetically coupled to the $S = {}^1/_2$ of the monoradical dianion corrole [Fe(III)Cl-corrole$^{+\bullet}$]. We show here that iron corroles as well as xanthene-modified and hangman xanthene iron corroles are redox active and catalyze the disproportionation of hydrogen peroxide via the catalase reaction, and that this activity scales with the oxidation potential. The meso position of corrole macrocycle is susceptible toward nucleophilic attack during catalase turnover. The reactivity of peroxide within the hangman cleft reported here adds to the emerging theme that corroles are good at catalyzing two-electron activation of the oxygen−oxygen bond in a variety of substrates.

Introduction

The proton-coupled electron transfer (PCET) chemistry that is essential to small molecule activation is achieved by hangman macrocycles by positioning a proton-donor/acceptor group from the scaffold of a xanthene backbone over the macrocyclic redox-active site.[1−4] The presence of a proton transfer group over the active site of a redox platform permits proton and electron transfer to be coupled in the process of activating molecules bound within the hangman cleft. The hangman construct is especially effective for oxygen−oxygen bond activation because the delivery of a proton from the hanging group promotes the two-electron heterolytic cleavage of the O−O bond.[1,2,4−9] Heretofore, the hangman motif has emphasized porphyrin[10−14] and salen[15,16] macrocycles. We have expanded the applicability of the hangman construct by developing methods to deliver hangman corrole xanthene (HCX).[17] Corroles, when compared to porphyrins, lack one meso bridge carbon atom and hence have a smaller macrocycle cavity. Moreover, the four macrocycle nitrogens bear three protons, as compared to only two in porphyrins and thus, when deprotonated, corroles have a higher charge, and they are able to stabilize metals in higher oxidation states.[18,19] Although the formal oxidation state of iron in metallocorrole is high, it does not necessarily describe the actual metal electron count. For instance, iron chloride corrole complexes may be described as either [Fe(IV)Cl-corrole] or [Fe(III)Cl-corrole$^{+\bullet}$]. Since both formulations lead to triplet ground states with rather similar spectroscopic

*To whom correspondence should be addressed. E-mail: nocera@mit.edu.

(1) Rosenthal, J.; Nocera, D. G. *Acc. Chem. Res.* **2007**, *40*, 543–553.
(2) Rosenthal, J.; Nocera, D. G. *Prog. Inorg. Chem.* **2007**, *55*, 483–544.
(3) Chang, C. J.; Chang, M. C. Y.; Damrauer, N. H.; Nocera, D. G. *Biochim. Biophys. Acta* **2004**, *1655*, 13–28.
(4) Reece, S. Y.; Hodgkiss, J. M.; Stubbe, J.; Nocera, D. G. *Philos. Trans. R. Soc. B* **2006**, *361*, 1351–1364.
(5) Chang, C. J.; Chng, L. L.; Nocera, D. G. *J. Am. Chem. Soc.* **2003**, *125*, 1866–1876.
(6) Liu, S.-Y.; Soper, J. D.; Yang, J. Y.; Rybak-Akimova, E. V.; Nocera, D. G. *Inorg. Chem.* **2006**, *45*, 7572–7574.
(7) Yang, J. Y.; Nocera, D. G. *J. Am. Chem. Soc.* **2007**, *129*, 8192–8198.
(8) Yang, J. Y.; Nocera, D. G. *Tetrahedron Lett.* **2008**, *49*, 4796–4798.
(9) Yang, J. Y.; Nocera, D. G. *ChemSusChem.* **2008**, *1*, 941–949.
(10) Chng, L. L.; Chang, C. J.; Nocera, D. G. *Org. Lett.* **2003**, *5*, 2421–2424.
(11) McGuire, R., Jr.; Dogutan, D. K.; Teets, T. S.; Suntivich, J.; Shao-Horn, Y.; Nocera, D. G. *Chem. Sci.* **2010**, *1*, 411–414.
(12) Chang, C. J.; Yeh, C.-Y.; Nocera, D. G. *J. Org. Chem.* **2002**, *67*, 1403–1406.
(13) Yeh, C.-Y.; Chang, C. J.; Nocera, D. G. *J. Am. Chem. Soc.* **2001**, *123*, 1513–1514.
(14) Dogutan, D. K.; Bediako, D. K.; Teets, T. S.; Schwalbe, M.; Nocera, D. G. *Org. Lett.* **2010**, *12*, 1036–1039.
(15) Liu, S.-Y.; Nocera, D. G. *J. Am. Chem. Soc.* **2005**, *127*, 5278–5279.
(16) Yang, J. Y.; Bachmann, J.; Nocera, D. G. *J. Org. Chem.* **2006**, *71*, 8706–8714.
(17) Dogutan, D. K.; Stoian, S.; McGuire, R. Jr.; Schwalbe, M. S.; Teets, T. S.; Nocera, D. G. *J. Am. Chem. Soc.* **2010**, *132*, 131−140.
(18) Gross, Z.; Gray, H. B. *Comments Inorg. Chem.* **2006**, *27*, 61–72.
(19) Wasbotten, I.; Ghosh, A. *Inorg. Chem.* **2006**, *45*, 4910–4913.

 Published on Web 01/18/2011

properties, a combined experimental and theoretical analysis is often required to differentiate between the two possible configurations.[20] Short Fe−N distances and an unperturbed macrocyclic scaffold in pentafluorophenyl and octaethyl corroles support a Fe(IV)-corrole formulation.[21−24] Subsequent studies have revised this view.[20,25−29] Chemical shifts of the ^{1}H NMR signals, EPR spectra of reduced species, magnetic susceptibility measurements, ^{57}Fe Mössbauer spectroscopy, and theoretical calculations of corrolates support the radical dianion state of the corrole macrocycle and an intermediate-spin ferric center.

We report here the preparation of xanthene-modified corroles (XC) and HCX macrocycles of iron and show that these species possess a redox non-innocent XC and HCX ligand. ^{57}Fe Mössbauer spectroscopy in conjunction with Density Functional Theory (DFT) calculations indicate that these iron chloride xanthene corroles are best described as [Fe(III)Cl-corrole$^{+\bullet}$].[20,30] The redox chemistry of iron chloride XC and HCX platforms has been exploited to drive the catalytic dismutation of hydrogen peroxide. The turnover frequency of the initial dismutation reaction indicates the ease of the reduction of the high valent iron oxo corrole.

Experimental Section

General Methods. Silica gel for column chromatography was obtained from Whatman Inc. (Silica Gel 60, 230−400 μm mesh). All solvents (tetrahydrofuran (THF), toluene, dichloromethane (DCM), dimethylformamide (DMF), hexane, and methanol) and most starting materials were obtained from Sigma-Aldrich and used without further purification. Compounds **1**,[12] **2**,[12] **3a**−**3c**,[31] **5a**,[17] and **6a**[17] were prepared according to literature procedures.

^{1}H NMR spectra were recorded at ambient temperature on a Varian Mercury 300 or 500 MHz spectrometer. All spectra were referenced to tetramethylsilane (TMS) or deuterated chloroform ($CDCl_3$) as an internal standard (measured values for δ are given in parts per million (ppm) and for J in Hertz (Hz)). Elemental analysis was performed by Midwest Microlab Laboratories, Indiana. Electrospray ionization (ESI) mass spectra were obtained using a Bruker Daltonics APEXIV 4.7 T FT-ICR-MS instrument at the DCIF facility of MIT. Matrix-assisted laser desorption/ionization-time of flight (MALDI-TOF) spectra were recorded on a Bruker Omniflex instrument with a reflectron accessory.

Absorption spectral measurements were made on DCM solutions of each compound using a Cary 5000 UV−vis−NIR spectrometer from Varian employing the software Cary WinUV. Quartz cells with a 10 mm path length were used. Steady state emission spectra were recorded on an automated Photon Technology International (PTI) QM 4 fluorimeter equipped with a 150-W Xe arc lamp and a Hamamatsu R928 photomultiplier tube. Excitation light was wavelength selected with glass filters. Solution samples for absorption and emission experiments were prepared under ambient conditions in DCM and contained in screw-cap quartz fluorescence cells. Lifetime measurements were performed on THF solutions prepared under nitrogen atmosphere and then subject to freeze-pump cycles.

10-(4-(5-Bromo-2,7-di-*tert*-butyl-9,9-dimethylxanthenyl))-5,15-bis(*tert*-butyl-phenyl) Corrole (4a). Method 1. Bromoxanthene aldehyde **1** (129 mg, 0.30 mmol) and 4-*tert*-butylphenyldipyrromethane **3a** (209 mg, 0.75 mmol) were dissolved in 10 mL of DCM. The condensation reaction commenced with the addition of 10 mL of 1.3 mM solution of TFA in DCM followed by stirring at room temperature for 7 h. 2,3-Dichloro-5,6-dicyano-1,4-benzoquinone (DDQ, 170 mg, 0.75 mmol) was then added, and the reaction mixture was stirred for an additional 15 min. The solution was loaded directly onto a silica gel column and eluted with DCM, and the first luminescent band was collected. Further purification by column chromatography on silica was accomplished using DCM/hexane (4:5). The resulting dark violet solid was suspended in methanol, filtered and dried in vacuo (58 mg, 20% yield based on **1**). ^{1}H NMR (500 MHz, $CDCl_3$, 25 °C): δ = 8.97 (d, J = 4.0 Hz, 2H), 8.89 (d, J = 5.0 Hz, 2H), 8.65 (s(br), 2H), 8.51 (d, J = 4.5 Hz, 2H), 8.35 (s(br), 4H), 8.04 (d, J = 2.5 Hz, 1H), 7.83 (d, J = 8.5 Hz, 4H), 7.80 (d, J = 2.5 Hz, 1H), 7.42 (d, J = 2.5 Hz, 1H), 7.10 (d, J = 2.5 Hz, 1H), 1.90 (s, 6H), 1.59 (s, 18H), 1.53 (s, 9H), 1.27 (s, 9H). HR(ESI)-MS (MH^+) (M = $C_{62}H_{65}N_4OBr$): Calcd m/z = 963.4429, found 963.4404. MS(MALDI-TOF) (M^+): 962.45. UV−vis, nm ($\varepsilon \times 10^{-3}$ M^{-1} cm^{-1}): 421 (132), 568 (17), 617 (15), 650 (14) in DCM. Anal. Calcd for $C_{62}H_{65}N_4OBr \cdot 0.5H_2O$: C, 76.68; H, 6.85; N, 5.77. Found: C, 76.50; H, 6.90; N, 5.65.

10-(4-(5-Bromo-2,7-di-*tert*-butyl-9,9-dimethylxanthenyl))-5,15-bismesityl corrole (4b). Method 1 was followed by using **3b** (198 mg, 0.75 mmol) in place of **3a**. Two column chromatographs (silica, ethylacetate/hexane = 1:25) afforded a violet solid, which was washed with methanol and dried in vacuo to furnish a purple solid (64 mg, 23% yield based on **1**). ^{1}H NMR (300 MHz, $CDCl_3$, 25 °C): δ = 8.87 (d, J = 4.2 Hz, 2H), 8.42 (m, 4H), 8.32 (d, J = 4.2 Hz, 2H), 8.00 (d, J = 2.4 Hz, 1H), 7.76 (d, J = 2.4 Hz, 1H), 7.37 (d, J = 2.1 Hz, 1H), 7.25 (m, 4H), 7.03 (d, J = 2.1 Hz, 1H), 2.59 (s, 6H), 1.99 (s, 6H), 1.91 (s, 6H), 1.86 (s, 6H), 1.49 (s, 9H), 1.23 (s, 9H). HR(ESI)-MS (MH^+) (M = $C_{60}H_{61}N_4OBr$): Calcd m/z = 933.4102, found 933.3979. MS(MALDI/TOF) (M^+): 932.57. UV−vis, nm ($\varepsilon \times 10^{-3}$ M^{-1} cm^{-1}): 409 (125), 424 (109), 567 (14), 603 (11), 634 (7) in DCM. Anal. Calcd for $C_{60}H_{61}N_4OBr$: C, 77.15; H, 6.58; N, 6.00. Found: C, 76.91; H, 6.52; N, 5.86.

10-(4-(5-Bromo-2,7-di-*tert*-butyl-9,9-dimethylxanthenyl))-5,15-bis(pentafluorophenyl) corrole (4c). Method 1 was followed by using **3c** (234 mg, 0.75 mmol) in place of **3a**. Column chromatography (silica, DCM/hexane = 1:2) afforded a dark purple solid, which was washed with methanol and dried in vacuo (72 mg, 24% yield based on **1**). ^{1}H NMR (500 MHz, $CDCl_3$, 25 °C): δ = 9.12 (d, J = 4.0 Hz, 2H), 8.68 (m, 4H), 8.57 (s(br), 2H), 8.02 (d, J = 2.5 Hz, 1H), 7.85 (d, J = 2.5 Hz, 1H), 7.40 (d, J = 2.5 Hz, 1H), 7.06 (d, J = 2.5 Hz, 1H), 1.89 (s, 6H), 1.54 (s, 9H), 1.24 (s, 9H). HR(ESI)-MS (MH^+) (M = $C_{54}H_{39}F_{10}N_4OBr$): Calcd for m/z = 1029.2220, found 1029.2242. MS(MALDI/TOF) (MH^+): 1030.37. UV−vis, nm ($\varepsilon \times 10^{-3}$ M^{-1} cm^{-1}): 414 (134), 560 (21), 612 (12) in DCM. Anal. Calcd for $C_{54}H_{39}F_{10}N_4OBr \cdot H_2O$: C, 61.90; H, 3.94; N, 5.35. Found: C, 62.07; H, 3.91; N, 5.24.

General Synthesis of FeCl Corroles 8. Method 2. A solution of **4** (0.15 mmol) and $FeCl_2$ (380 mg, 3.00 mmol) in 20 mL of dimethylformamide (DMF) was degassed with argon for 20 min.

(20) Ye, S.; Tuttle, T.; Bill, E.; Simkhovich, L.; Gross, Z.; Thiel, W.; Neese, F. *Chem.—Eur. J.* **2008**, *14*, 10839–10851.
(21) Caemelbecke, E. V.; Will, S.; Autret, M.; Adamian, V. A.; Lex, J.; Gisselbrecht, J.-P.; Gross, M.; Vogel, E.; Kadish, K. M. *Inorg. Chem.* **1996**, *35*, 184–192.
(22) Simkhovich, L.; Galili, N.; Saltsman, I.; Goldberg, I.; Gross, Z. *Inorg. Chem.* **2000**, *39*, 2704–2705.
(23) Simkhovich, L.; Goldberg, I.; Gross, Z. *Inorg. Chem.* **2002**, *41*, 5433–5439.
(24) Simkhovich, L.; Gross, Z. *Inorg. Chem.* **2004**, *43*, 6136–6138.
(25) Cai, S.; Licoccia, S.; D'Ottavi, C.; Paolesse, R.; Nardis, S.; Bulach, V.; Zimmer, B.; Kh. Shokhireva, T.; Walker, F. A. *Inorg. Chim. Acta* **2002**, *339*, 171–178.
(26) Zakharieva, O.; Schünemann, V.; Gerdan, M.; Licoccia, S.; Cai, S.; Walker, F. A.; Trautwein, A. X. *J. Am. Chem. Soc.* **2002**, *124*, 6636–6648.
(27) Cai, S.; Walker, F. A.; Licoccia, S. *Inorg. Chem.* **2000**, *39*, 3466–3478.
(28) Nardis, S.; Paolesse, R.; Licoccia, S.; Fronczek, F. R.; Vicente, M. G. H.; Shokhireva, T. K.; Cai, S.; Walker, F. A. *Inorg. Chem.* **2005**, *44*, 7030–7046.
(29) Walker, F. A.; Licoccia, S.; Paolesse, R. *J. Inorg. Biochem.* **2006**, *100*, 810–837.
(30) Steene, E.; Wondimagegn, T.; Ghosh, A. *J. Phys. Chem. B* **2001**, *105*, 11406–11413.
(31) Laha, J. K.; Dhanalekshmi, S.; Taniguchi, M.; Ambroise, A.; Lindsey, J. S. *Org. Process Res. Dev.* **2003**, *7*, 799–812.

Subsequent heating to reflux (110−120 °C) for 4 h resulted in a color change from dark green to dark red. This reaction can also be conducted in a microwave on a solution of 3 mL of DMF for 45 min at 120 °C. DMF was removed under vacuum, and the resulting product was dissolved in 30 mL of DCM. This solution was washed with water and brine to remove residual DMF, dried over Na_2SO_4, and concentrated to dryness. The resulting crude product was chromatographed (silica, diethylether) to afford the corresponding hangman μ-oxo dimer as a major brown band. The collected fraction was concentrated to dryness, and DCM (30 mL) and 7% HCl(aq) (10 mL) were added. The mixture was stirred vigorously for several hours. The organic phase was washed with water and brine, and dried over Na_2SO_4. The resulting solution was concentrated to dryness, and the resulting product was suspended in methanol, filtered, and dried in vacuum.

10-(4-(5-Bromo-2,7-di-*tert*-butyl-9,9-dimethylxanthenyl))-5,5-bis(*tert*-butylphenyl)corrolato Iron Chloride (8a). Yield: 99 mg (63%). HR(ESI)-MS (M^+) (M = $C_{62}H_{62}N_4OBrFe$): Calcd for m/z = 1015.3467, found 1015.3442 (major peak; a minor peak was observed at 1048.37). MS(MALDI/TOF) (M^+): 1015.37. UV−vis, nm ($\varepsilon \times 10^{-3}$ M^{-1} cm^{-1}): 360 (52), 418 (57), 637 (5.1) in DCM. Anal. Calcd for $C_{62}H_{62}N_4OBrClFe$: C, 70.89; H, 5.95; N, 5.33. Found: C, 70.64; H, 6.03; N, 5.37.

10-(4-(5-Bromo-2,7-di-*tert*-butyl-9,9-dimethylxanthenyl))-5,15-bismesityl-corrolato Iron Chloride (8b). Yield: 106 g (69%). HR(ESI)-MS (M^+) (M = $C_{60}H_{58}N_4OBrFe$): Calcd for m/z = 987.3154, found 987.3164 (major peak; a minor peak was observed at 1022.2866). MS(MALDI/TOF) $(M+Cl)^+$: 1022.19. UV−vis, nm ($\varepsilon \times 10^{-3}$ M^{-1} cm^{-1}): 362 (38), 389 (42), 625 (3.6) in DCM. Anal. Calcd for $C_{60}H_{58}N_4OBrClFe \cdot 1.5H_2O$: C, 68.67; H, 5.86; N, 5.34. Found: C, 68.87; H, 6.01; N, 5.10.

10-(4-(5-Bromo-2,7-di-*tert*-butyl-9,9-dimethylxanthenyl))-5,15-bis(pentafluorophenyl)corrolato Iron Chloride (8c). Yield: 121 mg (72%). HR(ESI)-MS (M^+) (M = $C_{54}H_{36}N_4OBrF_{10}Fe$): Calcd for m/z = 1083.1242, found 1083.1272 (major peak; a minor peak was observed at 1120). MS(MALDI/TOF) $(M+Cl)^+$: 1118.12. UV−vis, nm ($\varepsilon \times 10^{-3}$ M^{-1} cm^{-1}): 367 (48), 395 (53), 623 (4.8) in DCM. Anal. Calcd for $C_{54}H_{36}N_4OBrClF_{10}Fe \cdot H_2O$: C, 57.09; H, 3.37; N, 4.93. Found: C, 56.93; H, 3.41; N, 4.80.

10-(4-(5-Bromo-2,7-di-*tert*-butyl-9,9-dimethylxanthenyl))-5,15-bis(*tert*-butylphenyl)corrolato Iron-μ-oxo Dimer (7a). Dimer **7a** was obtained by stirring a solution of **8a** in dichloromethane vigorously overnight with a 0.1 M aqueous solution of NaOH. Subsequent extraction with water and brine, followed by drying the organic phase over $NaSO_4$ and removal of solvent to dryness yields **7a** in almost quantitative yield. HR(ESI)-MS (MH^+) (M = $C_{124}H_{124}N_8O_3Br_2Fe_2$): Calcd for m/z = 2046.6964, found 2046.6960. MS(MALDI/TOF) $(MH)^+$: 2046.35. UV−vis, nm ($\varepsilon \times 10^{-3}$ M^{-1} cm^{-1}): 388 (105), 518 (19) in DCM.

10-(4-(5-Carboxy-2,7-di-*tert*-butyl-9,9-dimethylxanthenyl))-5,15-bis(*tert*-butylphenyl)corrolato Iron Chloride (9a). Method 2 was followed with **6a** as the starting material. Purification with column chromatography (silica, DCM:EtOAc (2:1)) gave 98 mg (65%) of **9a**. HR(ESI)-MS (M^+) (M = $C_{63}H_{63}N_4O_3Fe$): Calcd for m/z = 979.4259, found 979.4240. MS(MALDI/TOF) (M^+): 979.49 UV−vis, nm ($\varepsilon \times 10^{-3}$ M^{-1} cm^{-1}): 360 (39.5), 419 (41.5), 638 (3.5) in DCM. Anal. Calcd for $C_{63}H_{63}N_4O_3ClFe$: C, 74.51; H, 6.25; N, 5.52. Found: C, 74.42; H, 6.38; N, 5.48.

5,10,15-Trismesitylcorrolato Iron Chloride. Method 2 was followed with 5,10,15-trimesitylcorrole as starting material. Purification by column chromatography (silica, DCM, DCM: methanol (24:1)) gave 79 mg (71%) of product. HR(ESI)-MS (M^+) (M = $C_{46}H_{41}N_4Fe$): Calcd for m/z = 705.6894, found 705.2561. MS(MALDI/TOF) (MCl): Calcd for $C_{46}H_{41}N_4FeCl$ m/z = 740.2369, found, 740.38, found (M^+) 705.31. UV−vis, nm ($\varepsilon \times 10^{-3}$ M^{-1} cm^{-1}): 361 (35.5), 387 (38), 625 (2.8).

10-(4-(5-Bromo-2,7-di-*tert*-butyl-9,9-dimethylxanthenyl))-5,15-bis(*tert*-butylphenyl)-5-hydroxo Isocorrole (10). 10 was isolated as a side product in less than 5% yield after work up of a crude reaction mixture during the synthesis of **7a**. Crude **4a** (0.15 mmol) and $FeCl_2$ (380 mg, 3.0 mmol) in 3 mL of DMF were reacted for 1 h at 120 °C in a microwave. DCM (30 mL) was added, and the solution was washed four times with water to remove residual DMF. The resulting organic fraction was stirred vigorously with 30 mL of 1 M NaOH (aq) overnight. The organic fraction was washed with water and brine and concentrated to dryness. Subsequent column chromatography (silica, DCM) afforded μ-oxo dimer **7a** as a first major brown band. A smaller green band appeared behind the first band, and it was collected separately. Further purification on a second column (silica, DCM:hexane (2:1)) afforded pure **10**. HR(ESI)-MS (M^+) (M = $C_{62}H_{65}N_4O_2Br$): Calcd for m/z = 977.4364, found 977.4326. MS(MALDI/TOF) (M): 978.56. UV−vis, nm ($\varepsilon \times 10^{-3}$ M^{-1} cm^{-1}): 407 (42), 683 (6.4) in DCM.

X-ray Crystallographic Details. The crystals were mounted on a Bruker three circle goniometer platform equipped with an APEX 2 detector. A graphite monochromator was employed for wavelength selection of the Cu Kα radiation (λ = 1.54178 Å, isocorrole **10**) or Mo Kα radiation (λ = 0.71073 Å, Corrole(Mes)$_3$FeCl and **8a**). The data were processed and refined using the program SAINT supplied by Siemens Industrial Automation. Structures were solved by direct methods in SHELXS and refined by standard difference Fourier techniques in the SHELXTL program suite (6.10 v., Sheldrick G. M., and Siemens Industrial Automation, 2000). Hydrogen atoms bound to carbon were placed in calculated positions using the standard riding model and refined isotropically. Hydrogen atoms bound to nitrogen or oxygen were located in the difference map and refined semifreely; all non-hydrogen atoms were refined anisotropically. The structure of Corrole(Mes)$_3$FeCl contained solvent molecules which were modeled as two-part disorders. The 1−2 and 1−3 distances of all disordered parts were restrained to be similar using the SADI command; the rigid-bond restraints SIMU and DELU were also used on disordered parts. The crystal of **10** was found to be partially disordered, and a heavily disordered solvent molecule was removed using the SQUEEZE operation in PLATON.[32]

Crystallographic Data for 8a. $C_{62}H_{62}N_4OBrClFe \cdot 2C_6H_6$, M = 1206.58, green crystals, monoclinic, space group $P2_1/n$, a = 15.746(2) Å, b = 13.8863(19) Å, c = 29.932(4) Å, α = 90.00°, β = 99.118(2)°, γ = 90.00°, V = 6462.1(15) Å^3, Z = 4, T = 100(2) K, R_1 = 0.0785, wR_2 = 0.1884, GOF = 1.052.

Crystallographic Data for 10. $C_{62}H_{65}N_4O_2Br$, M = 978.09, green crystals, triclinic, space group $P\bar{1}$, a = 6.10300(10) Å, b = 14.2694(3) Å, c = 33.1609(6) Å, α = 85.023(2)°, β = 89.002(2)°, γ = 85.403(2)°, V = 2867.55(9) Å^3, Z = 2, T = 100(2) K, R_1 = 0.0792, wR_2 = 0.1856, GOF = 1.148.

Crystallographic Data for Corrole(Mes)$_3$FeCl. $C_{46}H_{41}N_4ClFe \cdot C_6H_{12} \cdot C_6H_6$, M = 902.38, green crystals, monoclinic, space group $P2_1/n$, a = 11.9567(12) Å, b = 20.250(2) Å, c = 20.050(2) Å, α = 90.00°, β = 99.108(2)°, γ = 90.00°, V = 4793.3(8) Å^3, Z = 4, T = 100(2) K, R_1 = 0.0693, wR_2 = 0.1856, GOF = 1.034.

Cyclic Voltammetry. All cyclic voltammograms (CV) were performed on DCM solutions containing 0.1 M NBu_4PF_6 (tetrabutylammonium hexafluorophosphate) and the corrole compound under argon atmosphere at ambient temperature. A potentiostat/galvanostat from CH Instruments was used to record CVs. A three compartment cell was outfitted with a 0.07 cm^2 glassy carbon button electrode as the working electrode, a platinum wire as the auxiliary electrode, and Ag/AgCl as the reference electrode. Reported potentials were referenced to a ferrocenium/ferrocene (Fc^+/Fc) internal standard. CVs were collected at scan rates of 10−100 mV/s.

Spectroscopy. Samples for transient emission were contained within high-vacuum cells consisting of a 2-mm path length clear fused-quartz cell, which was connected to a 10-cm^3 solvent reservoir via a graded seal. The two chambers were isolated

(32) Sluis, P. v. d.; Spek, A. L. *Acta Crystallogr.* **1990**, *A46*, 194–201.

Scheme 1

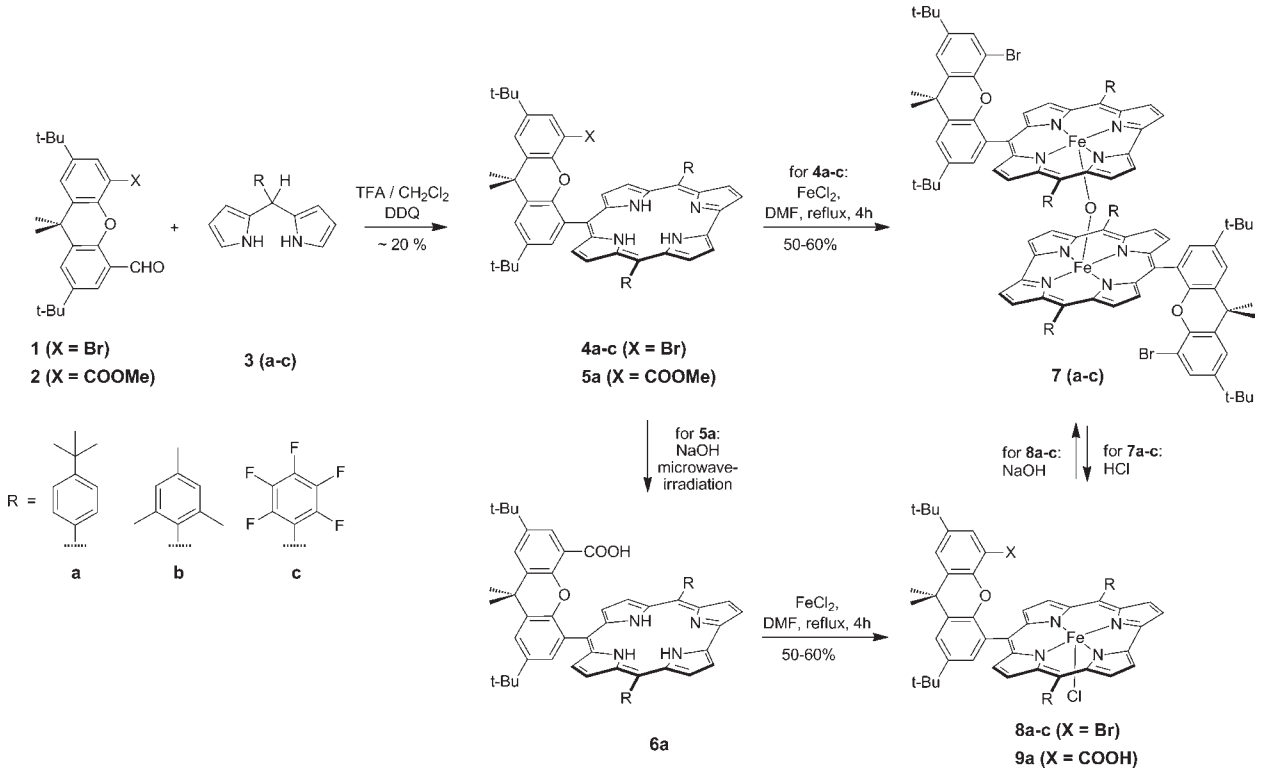

from the environment and from each other by high-vacuum Teflon valves. An aliquot of 100 μL of sample dissolved in dry THF was added to the cell. The THF in the reservoir was subject to three freeze−pump−thaw cycles (10^{-6} Torr) and transferred back to the cell by vacuum transfer.

Excitation of the samples was accomplished with the output of a 45 fs Coherent Libra HE operating at 1 kHz to produce 4 mJ of 800 nm light. Visible wavelengths were generated using a Coherent OPerA Solo tunable over the entire visible range of the spectrum, with pulse energies of approximately 20 μJ. Average excitation power at the sample was attenuated to 5 μJ to avoid photodamage. Transient emission lifetime kinetics were measured on a Hamamatsu C4334 Streak Scope streak camera (2D, *y*-axis is time and the *x*-axis is nm). The emission was collected at the magic angle (θ = 54.7°) over a 20 to 50 ns time window where the spectral axis (100-nm range) was centered on the emission peak.

Variable-field, variable-temperature Mössbauer spectra were recorded in the temperature range from 4.2−180.0 K and magnetic fields up to 8.0 T using a constant acceleration spectrometer fitted with a liquid helium cooled Janis Research Super-Varitemp cryostat and a superconducting magnet. Spectral simulations were performed using the WMOSS software (Edina, MN). The isomer shifts are quoted relative to iron metal at room temperature.

Density Functional Theory (DFT). Computations were carried out using the quantum-chemical software package Gaussian 09.[33] To investigate the electronic structure of **8a**, a simplified structural model was constructed in which the methyl and 4-*tert*-butyl side groups of the xanthene backbone were replaced with hydrogen atoms and the *tert*-butyl groups of the 4-*tert*-butylphenyl−meso substituents were replaced with methyl groups. Geometry optimization and single point calculations were performed with the B3LYP/6-311 g hybrid functional/basis set combination.[34,35] Details of the calculation are provided in the Supporting Information. The stability of the ground state was tested by time-dependent (TD) DFT. Electronic charge and spin distributions were monitored with Mulliken population analysis. The ^{57}Fe isomer shift was calculated using the calibration given by Vrajmasu et al.;[36] electric field gradient (EFG) parameters ΔE_Q and η, as well as the A^{FC} and A^{SD} of the hyperfine coupling tensor were evaluated with the properties modules of the Gaussian 09 program.

Catalytic Assay. Hydrogen peroxide dismutation reactions were performed at room temperature in a sealed (PTFE septum) 20 mL reaction vial equipped with a magnetic stirbar and a capillary gas delivery tube linked to a graduated buret filled with water. The reaction vial was charged with 2 mmol of the iron corrole catalyst, 50 mmol of 1,5-dicyclohexylimidazole, 3.0 mL of CH_2Cl_2, and 1.0 mL of CH_3OH. The dicyclohexylimidazole is used as a ligand to axially coordinate iron opposite the hangman cleft. The solution was stirred for 5−10 min to ensure gas pressure equilibration. An aliquot of 10.4 M (30%) aqueous H_2O_2 (0.2 mL) was added to the reaction mixture via syringe, and the reaction mixture was stirred vigorously. The time was set to zero immediately after addition of H_2O_2. The O_2 evolution reaction was monitored volumetrically, and the TON for produced O_2 (n) was calculated using the ideal gas equation. The identity of the oxygen gas was confirmed independently by gas chromatography.

Results and Discussion

Synthesis and Characterization. Free base and iron XC and HCX complexes were prepared by the synthetic strategy outlined in Scheme 1. These corroles are delivered in a streamlined condensation reaction that we have previously reported.[17] Briefly, xanthene dibromide (or monobromo-monomethoxycarbonyl xanthene) was converted into bromoxanthene aldehyde **1** (respectively **2**) by lithiation followed by reaction with DMF.[12] Substituted dipyrromethanes

(33) *Gaussian 09*, Revision A2; Gaussian, Inc.: Wallingford, CT, 2009; full citation in the Supporting Information.
(34) Becke, A. D. *J. Chem. Phys.* **1993**, *98*, 1372–1377.
(35) Lee, C.; Yang, W.; Parr, R. G. *Phys. Rev. B* **1998**, *37*, 785–789.
(36) Vrăjmaşu, V. V.; Münck, E.; Bominaar, E. L. *Inorg. Chem.* **2003**, *42*, 5974–5988.

(R = 4-*tert*-butylphenyl (**3a**), mesityl (**3b**), and pentafluorophenyl (**3c**) were synthesized by the Lindsey method of condensing commercially available pyrrole and aryl aldehydes.[31,37] The condensation of **1** or **2** with the corresponding aryl dipyrromethane in dichloromethane/trifluoroacetic acid mixture furnishes the xanthene corrole compounds in about 20% yield (Supporting Information, Table S1) under optimized conditions, which were ascertained from the 4-*tert*-butylphenyl system to be 37.5 mM DPM, 15 mM **1**, 0.6 mM TFA, 7 h stirring at room temperature and quenching with 2,3-dichloro-5,6-dicyanobenzoquinone (DDQ entry 7, Supporting Information, Table S1). We note that concentrations of reactants and Lewis acid, which are lower than those usually employed in corrole synthesis, led to improved yields of the xanthene modified corroles (entries 1−7, Supporting Information, Table S1).[38] In addition, variation of the reaction conditions by using longer reaction times (entries 8 and 10, Supporting Information, Table S1), hydrochloric acid in a water−methanol mixture as a solvent (entries 9 and 10, Supporting Information, Table S1), or *p*-chloranil as an oxidizing agent (entry 4) did not improve the yield as has been found for other corrole compounds.[39]

^{1}H NMR spectra of the free base XC complexes (aryl = 4-*tert*-butylphenyl (**4a**), mesityl (**4b**), and pentafluorophenyl (**4c**)) show two sets of signals in the aromatic region between 7 and 9 ppm corresponding to four proton signals assignable to the xanthene backbone and four signals assignable to the corrole macrocycle (Supporting Information, Figures S7−S9). Additional proton signals in the aromatic region appear for the mesityl substituent (two singlets) and for the 4-*tert*-butylphenyl substituent (two multiplets). In the aliphatic region, signals are clearly distinguished for the two methyl and two 4-*tert*-butyl substituents of the xanthene backbone as well as one additional signal for the 4-*tert*-butyl groups on the macrocycle of **4a** and three signals for the methyl groups of **4b**. For the latter complex, the mesityl peaks are split owing to constricted rotation about the $C_{ipso}-C_{meso}$ bond of the aryl groups and lowered symmetry above and below the corrole plane that is imposed by the xanthene scaffold. Pyrrolic (3H) and carboxylic acid (1H) protons were not observed in ^{1}H NMR spectra recorded at room temperature.

Iron insertion was achieved by refluxing the free base **4** or **6a** with an excess of iron dichloride in DMF as previously described.[22] The iron chloride complexes (R = 4-*tert*-butylphenyl (**8a**, **9a**), mesityl (**8b**), and pentafluorophenyl (**8c**)) were isolated in 60% yield after purification by column chromatography. The presence of the paramagnetic iron center led to interpretable but very complex ^{1}H NMR spectra with signals in the −30 to +100 ppm region. The structure of the iron corrole complexes was, however, revealed by X-ray crystal analysis.

Compounds Corrole(Mes)$_3$FeCl[40] and Corrole(C_6F_5)$_3$FeCl[22] were prepared as reference systems to elucidate the influence of the xanthene backbone. Crystals of Corrole(Mes)$_3$FeCl were grown from a methanol/dichloromethane solution. Crystals of **8a** were obtained by slow evaporation of a benzene solution of the complex. The structures of **8a**

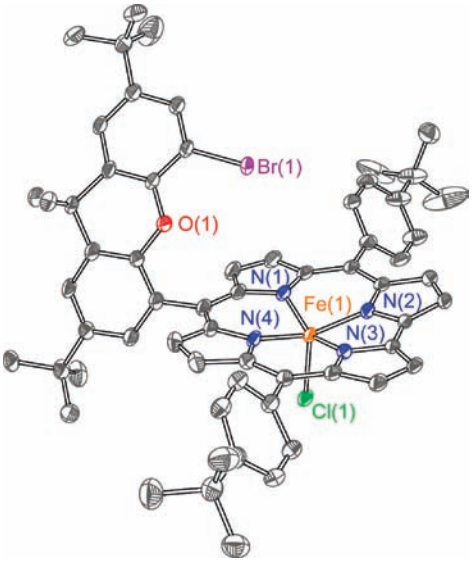

Figure 1. X-ray crystal structure of **8a**, with thermal ellipsoid plots shown at 50% probability level. Hydrogen atoms are omitted for clarity. Selected bond distances (Å) and angles (deg): Fe−N1 1.921, Fe−N2 1.901, Fe−N3 1.903, Fe−N4 1.928, Fe−Cl 2.245, N1−Fe−N3 153.6, N4−Fe−N2 154.2, N2−Fe−Cl 103.7, N4−Fe−Cl 101.5.

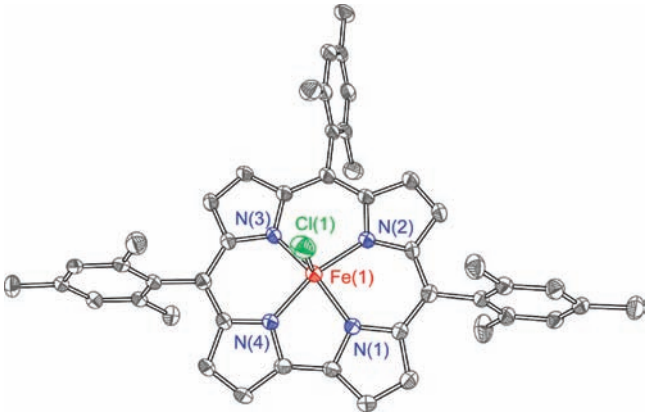

Figure 2. X-ray crystal structure of Corrole(Mes)$_3$FeCl, with thermal ellipsoid plots shown at 50% probability level. Hydrogen atoms are omitted for clarity.

and Corrole(Mes)$_3$FeCl are shown in Figures 1 and 2, respectively. Both compounds show similar structural features to known iron chloride corrole complexes.[28,41] The five coordinate iron center is considerably displaced above the N4-plane of the macrocycle, which has a slight saddle form (Figures 1 and 2). The distance of the Fe atom from the best-fit N4-plane is virtually identical in both structures: 0.4213(17) Å for Corrole(Mes)$_3$FeCl and 0.4181(21) Å for **8a**. The Fe−N distances for the two structures are nearly identical, ranging from 1.892(3) to 1.929(4) Å. These metrics are in accord with those observed for [Fe(tpfc)Cl] (tpfc = tris(pentafluorophenyl)corrole, Corrole(C_6F_5)$_3$FeCl) and [Fe(oec)Cl] with oec = octaethylcorrole,[21] which have nearly identical Fe−N distances and similar puckering of the Fe atom out of the N4-plane (0.367 Å). In the solid-state structure of **8a**, the xanthene backbone stands almost perpendicular to the macrocyclic plane, while the

(37) Dogutan, D. K.; Zaidi, H. S. H.; Thamyongkit, P.; Lindsey, J. S. *J. Org. Chem.* **2007**, *72*, 7701–7714.
(38) Gryko, D. T.; Jadach, K. *J. Org. Chem.* **2001**, *66*, 4267–4375.
(39) Koszarna, B.; Gryko, D. T. *J. Org. Chem.* **2006**, *71*, 3707–3717.
(40) Gryko, D. T.; Koszarna, B. *Org. Biomol. Chem.* **2003**, *1*, 350–357.
(41) Vogel, E.; Will, S.; Tilling, A. S.; Neumann, L.; Lex, J.; Bill, E.; Trautwein, A. X.; Wieghardt, K. *Angew. Chem., Int. Ed. Engl.* **1994**, *33*, 731–735.

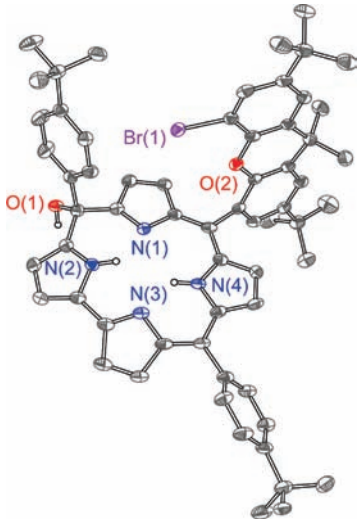

Figure 3. X-ray crystal structure of **10**, with thermal ellipsoid plots shown at 50% probability level. Hydrogen atoms bonded to carbon are omitted for clarity.

aryl substituents are twisted about 60° out of the macrocyclic plane. Excepting the axial chloride found opposite to the bromide of the xanthene scaffold, the overall hangman scaffold of **8a** and **9a** is similar to that for the hangman corrole framework, which has recently been published.[17] No cations or anions are present in either crystal structure; this observation is consistent with a *formal* Fe(IV) center.

MALDI-TOF-MS indicated the presence of a μ-oxo intermediate **7**, which was not typically isolated. This compound was transformed directly into **8** by treating a DCM solution of **7** with aqueous HCl. Only for the 4-*tert*-butylphenyl substituted XC dimer **7a** was the μ-oxo dimer isolated and characterized by standard analytical techniques. The NMR spectrum of **7a** shows signals in the expected range of 0 to 10 ppm in contrast to Fe(IV)Cl corrole compounds such as **8a** and **9a**, which show markedly shifted NMR signals (−45 to 30 ppm). A second corrole **10** could also be isolated from treating crude **8a** with sodium hydroxide. The crystal structure of **10** shown in Figure 3 reveals that OH attacks the carbon at the meso position of the corrole. Isocorrole formation from hydroxide[42] and alkoxide attack[43,44] is known to occur from the oxidized corrole macrocycle. This reaction sequence may also be envisioned for the formation of **10**. The resulting isocorrole framework exhibits similar metrics to that produced from an attempted demetalation of a corrolato silver complex.[42] The addition of the hydroxy group breaks the symmetry of the corrole macrocycle; the symmetry lowering is clearly observed in the ^{1}H NMR spectrum. All β-pyrrolic protons are inequivalent, and each gives rise to two sets of distinguishable ^{1}H resonances: four doublets and four doublet of doublets (^4J(N,H) = 2 Hz, see Supporting Information, Figure S10) appear in the region between 6 and 7 ppm, indicating that aromaticity is not

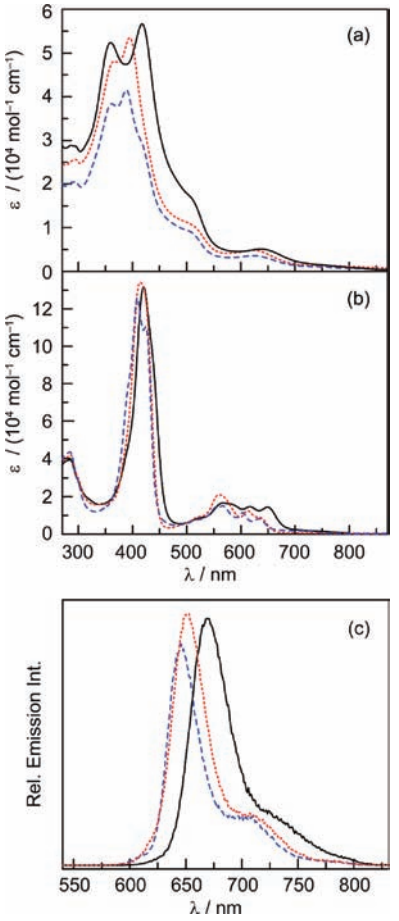

Figure 4. Electronic absorption spectra of the (a) iron XC (**8a** (solid line, black), **8b** (dashed line, blue), **8c** (dotted line, red) and (b) the 3H XC (**4a** (solid line, black), **4b** (dashed line, blue), **4c** (dotted line, red)) series in DCM. (c) Emission spectra of the 3H XC (**4a** (solid line, black), **4b** (dashed line, blue), **4c** (dotted line, red)) series in DCM.

longer maintained. Moreover, two single resonances are observed for the pyrrole N−H protons at 16.0 and 16.2 ppm and a distinct singlet for the O−H proton at 2.6 ppm. This observation contrasts that of the pyrrolic N−H protons of the parent complex **4**, which are not detected by ^{1}H NMR owing to their delocalization about the corrole core under conditions of fast exchange. As shown in Supporting Information, Figure S3 the localized pyrrole protons in **10** establish an extended array in the solid state structure via a hydrogen bond network.

Spectroscopy. The UV−vis absorption spectra of the corroles offer an interesting comparison to their porphyrin relatives. Figure 4a shows the absorption spectra of the iron XC series of compounds. The Soret band, centered about 420 nm, is split and has a considerably attenuated extinction coefficient when compared to those of analogous porphyrins (ca. 200,000 M^{-1} cm^{-1}). This splitting of the Soret band is attributed to the lower symmetry of the corrole macrocycle ring.[20,45] The $\lambda_{abs,max}$ of the series (see Table 1) follows the trend **8b** ∼ **8c** > **8a**. This trend stems from the twisting of the aryl substituents out of the macrocyclic plane as a result of steric demands exerted by the mesityl and pentafluorophenyl substituents in meso positions. As shown in

(42) Stefanelli, M.; Shen, J.; Zhu, W. H.; Mastroianni, M.; Mandoj, F.; Nardis, S.; Ou, Z. P.; Kadish, K. M.; Fronczek, F. R.; Smith, K. M.; Paolesse, R. *Inorg. Chem.* **2009**, *48*, 6879–6887.
(43) Nardis, S.; Pomarico, G.; Fronczek, F. R.; Vicente, M. G. H.; Paolesse, R. *Tetrahedron Lett.* **2007**, *48*, 8643–8646.
(44) Pomarico, G.; Xiao, X. A.; Nardis, S.; Paolesse, R.; Fronczek, F. R.; Smith, K. M.; Fang, Y. Y.; Ou, Z. P.; Kadish, K. M. *Inorg. Chem.* **2010**, *49*, 5766–5774.
(45) Shen, J.; El Ojaimi, M.; Chkounda, M.; Gros, C. P.; Barbe, J. M.; Shao, J.; Guilard, R.; Kadish, K. M. *Inorg. Chem.* **2008**, *47*, 7717–7727.

Table 1. Summary of the Photophysical Properties of Free Base and Iron XC Compounds

cmpd	$\lambda_{abs,max}$/nm ($\varepsilon/10^3$ M^{-1} cm^{-1}) [a]	$\lambda_{em,max}$/nm [b] CH_2Cl_2	$\lambda_{em,max}$/nm [b] THF	τ/nm [c]
4a	421 (132), 568 (17.0), 617 (15.0), 650 (14.0)	669	683	4.7
4b	409 (125), 424 (109), 567 (14.0), 603 (11.0), 634 (7.0)	646	657	5.2
4c	414 (134), 560 (21.0), 612 (12.0), 630 (8.6)	651	665	4.1
7a	388 (105), 518 (19.0)			
8a	360 (52.0), 418 (57.0), 637 (5.1)			
8b	362 (38.0), 389 (42.0), 625 (3.6)			
8c	367 (48.0), 395 (53.0), 623 (4.8)			
9a	360 (39.0), 419 (42.0), 636 (3.5)			

[a] Absorption maxima in dichloromethane at room temperature. [b] Emission maxima in indicated solvent at room temperature. [c] Emission lifetime of XC compound in THF that had been subject to freeze-pump thaw cycles to remove oxygen; measurements were performed at room temperature (λ_{exc} = 400 nm).

porphyrins, the twisting of the rings attenuates electronic coupling between the aromatic meso substituents and the macrocycle ring.[13,22,46,47] With the absence of ortho substituents on the 4-*tert*-butylphenyl ring of **8a**, this steric hindrance is removed, and electronic delocalization onto the aromatic rings from the corrole is possible, thus resulting in red-shifts of the Soret band. Spectral differences among the series in the Q-band region are less pronounced. We note that the Soret and the Q bands of the iron corroles (see Figure 4a for **8** and Supporting Information, Figure S1 for **7a**, respectively) exhibit a strong hypsochromic shift as well as a broadening and a lower absorption cross-section of the Soret band when compared to that of the free base corrole (Figure 4b), though hydroxylation also leads to attenuation of the Soret band (Supporting Information, Figure S2). Moreover, the electronic properties of the metalated and free base systems differ in one other important aspect. The absence of low-lying dd states in free base XC compounds removes efficient non-radiative decay pathways from the system; consequently, the free base XC corroles are luminescent (Figure 4c). The $\lambda_{em,max}$ of the series (Table 1) follows the same trend as that of the absorption spectra, **4b** ~ **4c** > **4a**. The emission spectra exhibit a noticeable red-shift of about 15 nm for the compounds dissolved in THF (see Table 1). The emission lifetime of the free base XC is about 4 ns in THF at room temperature under oxygen free conditions (see Table 1).

An authentic assignment of the oxidation state of the metal center is confounded by the redox non-innocence of the ligand. The formal Fe(IV)Cl formulation engenders a $S = 1$ triplet ground state. But the same spin multiplicity may be obtained for a Fe(III) corrole-radical formulation [$Fe^{III}Cl(corrole^{+\bullet})$], where the ferric ion has an intermediate spin configuration $S_{Fe} = {}^3/_2$ that is antiferromagnetically coupled to the $S_{corrole^{+\bullet}} = {}^1/_2$ spin of the oxidized corrole ligand. Direct exchange interactions between metal ions and ligand spins may be quite strong, typically in the range of hundreds if not thousands of wavenumbers.[48] DFT estimates for the magnitude of the putative $S_{Fe} = {}^3/_2$, $S_{corrole^{+\bullet}} = {}^1/_2$ exchange interaction $J = +1328$ cm^{-1} for [FeCl(tpfc)]. Magnetic susceptibility analysis yields the value $J = +544$ cm^{-1} for [FeCl(tpfc)] and $J \sim +350$ cm^{-1} for [FeCl(7,13-Me_2Et_6corr)], using the $J\mathbf{S}_1\cdot\mathbf{S}_2$ convention.[20,26] Therefore, both formulations give triplet ground states that are well isolated from excited states, and no definitive conclusion can be drawn about the nature of the ground state on the basis of spin quantum number alone.

Table 2. Zero Field Mössbauer Parameters of Complexes **7a**, **8a**−**c**, **9a** and Related FeCl Corrole Compounds[a]

compound	T/K	δ/mm s^{-1}	ΔE_Q/mm s^{-1}
8a	4.2	0.19	2.91
8b	4.2	0.18	2.84
8c	4.2	0.19	2.95
9a	4.2	0.20	2.97
[FeCl(tpfc)] [b]	80	0.18	2.94
[FeCl(tdcc)] [b]	80	0.19	2.88
[FeCl(7,13-Me_2Et_6corr)] [c]	4.2	0.21	3.02
[FeCl(OECorr)] [d]	77	0.19	2.99
7a	4.2	0.04	2.24
[(OECorr)Fe]$_2$(μ-O) [d]	77	0.02	2.35

[a] Tabulated values are limited to iron-corrole complexes that have either chloride or bridging oxo axial ligands. [b] Data taken from ref 20. [c] Data taken from ref 26. [d] Data taken from ref 41.

Mössbauer spectra recorded at 4.2 K in zero applied magnetic field for **7a**, **8a**−**c** and **9a** consist of similar quadrupole doublets, whose isomer shifts, δ, and quadrupole splittings, ΔE_Q, are listed in Table 2. Weak magnetic fields (< 0.1 T) have little effect on the spectra, which are consistent with zero or integer spin of systems with an even number of electrons. Variable-field, variable-temperature Mössbauer spectroscopy analysis was carried out for **8a**. A series of spectra were recorded at temperatures between 4.2 and 150 K in variable fields ranging from 0.0 to 8.0 T. These spectra were analyzed in the framework of an $S = 1$ spin Hamiltonian,

$$\hat{H} = D\left[\hat{S}_z^2 - \frac{2}{3} + \frac{E}{D}(\hat{S}_x^2 - \hat{S}_y^2)\right] + \beta\hat{\mathbf{S}}\cdot\mathbf{g}\cdot\mathbf{B} + \hat{\mathbf{S}}\cdot\mathbf{A}\cdot\hat{\mathbf{I}} + \beta_n g_n \hat{\mathbf{I}}\cdot B + \hat{H}_Q$$

$$\hat{H}_Q = \frac{eQV_{z'z'}}{12}\left[3\hat{I}_{z'}^2 - \frac{15}{4} + \eta(\hat{I}_{x'}^2 + \hat{I}_{y'}^2)\right]$$

$$\Delta E_Q = \frac{eQV_{z'z'}}{2}\sqrt{1 + \frac{\eta^2}{3}}$$

The choice of a spin state $S = 1$ is justified both by the room temperature magnetic moment of $\mu_{eff} = 2.83\,\mu_B$, as

(46) Palmer, J. H.; Mahammed, A.; Lancaster, K. M.; Gross, Z.; Gray, H. B. *Inorg. Chem.* **2009**, *48*, 9308–9315.
(47) Eikey, R. A.; Khan, S. I.; Abu-Omar, M. M. *Angew. Chem., Int. Ed.* **2002**, *41*, 3592–3595.
(48) Stoian, S. A.; Vela, J.; Smith, J. M.; Sadique, A. R.; Holland, P. L.; Münck, E.; Bominaar, E. L. *J. Am. Chem. Soc.* **2006**, *128*, 10181–10192.

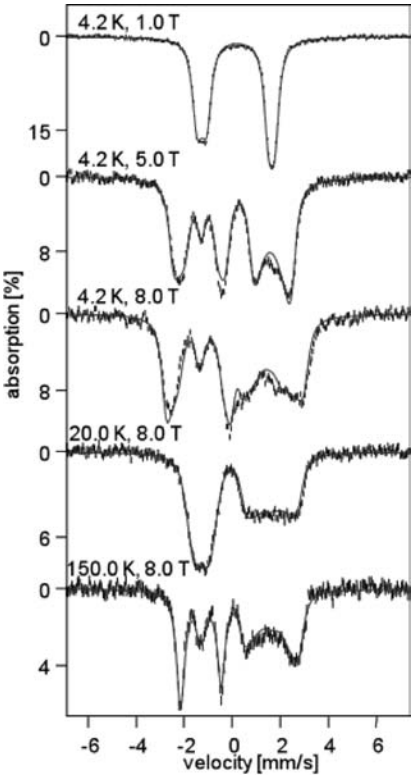

Figure 5. Variable-field, variable-temperature Mössbauer spectra of **8a** recorded for a ^{57}Fe enriched, solid state sample. The applied field is aligned parallel to the incident γ beam. The solid lines are best fits obtained using an $S = 1$ spin Hamiltonian with $D = 16.5$ cm^{-1}, $E/D = 0.12$, $g_x = g_y = g_z = 2.00$ $\delta = 0.193$ mm/s, $\Delta E_Q = 2.911$ mm/s, $\eta = 0.0$, $A_x = -24.0$ T, $A_y = -26.7$ T, $A_z = +1.0$ T and a rotated EFG tensor such that $\alpha_{EFG} = \gamma_{EFG} = 0.0°$, $\beta_{EFG} = 18.0°$.

determined by NMR using Evans method,[49] and by the similarity of the zero field Mössbauer parameters with those reported for other FeCl corrole complexes, which have been shown to have a $S = 1$ ground state.[20,26,41]

The hyperfine splitting observed in the 8.0 T, 150.0 K spectrum is dominated by the nuclear Zeeman and quadrupole interactions. The magnetic hyperfine interactions have a minor effect on the spectra because the thermal spin expectation value, $\langle S \rangle_{th} \sim 1/T$, and the associated internal field, $B_{int} = A \cdot \langle S \rangle_{th} / g_n \beta_n$, are small at this temperature. Under these conditions, the sign of ΔE_Q is unambiguously determined and found to be positive. Moreover, simulations of the 8.0 T, 100.0−150.0 K spectra yield an asymmetry parameter $\eta \approx 0$, implying that the electric field gradient (EFG) tensor is axial. The internal field of the 4.2 K spectra does not saturate even in strong applied fields up to 8.0 T. This behavior is generally found when the zero field splitting (ZFS) is large and positive and, in the present case, implies that the lowest sublevel of the spin multiplet is $|S = 1, M_S = 0\rangle$. The internal field results from mixing of the excited $|S = 1, M_S = \pm 1\rangle$ magnetic doublet into the ground sublevel by the applied field. These qualitative observations are supported by the spectral simulations shown in Figure 5. We find a hyperfine coupling tensor A that is quasi-axial with $|A_x| \sim |A_y| \gg |A_z|$. At 4.2 K, the simulated splitting and spectral pattern are strongly correlated with $A_{x,y}$, whereas A_z

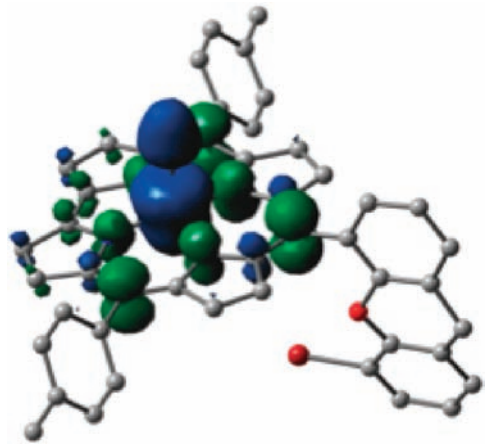

Figure 6. Spin-density plot calculated for the ground state of **8a**.

is a rather soft parameter. Fitting of the set of variable-field spectra yields the ZFS parameters $D = +16.5 \pm 0.5$ cm^{-1} and $E/D = 0.12 \pm 0.02$, and the hyperfine coupling constants $A_x = -24.0 \pm 0.2$ T, $A_y = -26.7 \pm 0.2$ T, and $A_z = +1.0 \pm 2.0$ T. While rather satisfactory simulations are obtained with EFG, A, and ZFS tensors of which the principal axes are collinear, further improvement in the fit is achieved by rotating the EFG tensor about the x-axis of ZFS with $\beta_{EFG} = 18°$ (see Supporting Information, Table S5), in particular in the representation of the low energy feature in the 7.0−8.0 T, 4.2 K spectra. We note that at 4.2 K and fields up to 8.0 T, the combined Boltzmann population of the excited doublet is less than 0.05, consequently the spectra calculated in fast or slow relaxation regime are identical.

Mössbauer spectra recorded for **7a** (Supporting Information, Figure S5) indicate that the bridging oxo ligand mediates a strong antiferromagnetic coupling between the two $S_{local} = 1$ local iron sites to yield a $S_{total} = 0$ ground state. Up to temperatures of 120 K, no evidence for the population of an excited state is observed. The isomer shift $\delta = 0.04$ mm/s of **7a** is lower than for the chloro iron corrolato complexes, indicating a higher Fe(IV) character in the former species. Complex **7a** has a positive $\Delta E_Q = +2.24$ mm/s and a small $\eta \approx 0.2$, values similar to those for **8a**.

The range of isomer shifts obtained for FeCl corrole complexes overlaps both with those reported for authentic $S_{Fe} = 1$ Fe(IV) species and of low-spin ferric compounds.[50−54] Therefore, to provide further aid in interpreting Mössbauer data, the electronic ground state of **8a** was examined with spin-unrestricted DFT calculations. The spin density plot calculated for the $S = 1$ ground state of the geometry-optimized model (Figure 6) reveals that the DFT solution is best described as a broken symmetry (BS) state with the majority spin (α, spin-up) localized on the [FeCl] moiety and the minority spin

(49) Garland, C. W.; Nibler, J. W. Shoemaker, D. P. *Experiments in Physical Chemistry*, 8th ed.; McGraw-Hill: New York: 2003, pp 371−379.

(50) Collins, T. J.; Fox, B. G.; Hu, Z. G.; Kostka, K. L.; Munck, E.; Rickard, C. E. F.; Wright, L. J. *J. Am. Chem. Soc.* **1992**, *114*, 8724–8725.

(51) Rohde, J. U.; In, J. H.; Lim, M. H.; Brennessel, W. W.; Bukowski, M. R.; Stubna, A.; Münck, E.; Nam, W.; Que, L. *Science* **2003**, *299*, 1037–1039.

(52) Justel, T.; Muller, M.; Weyhermuller, T.; Kressl, C.; Bill, E.; Hildebrandt, P.; Lengen, M.; Grodzicki, M.; Trautwein, A. X.; Nuber, B.; Wieghardt, K. *Chem.—Eur. J.* **1999**, *5*, 793–810.

(53) Kostka, K. L.; Fox, B. G.; Hendrich, M. P.; Collins, T. J.; Rickard, C. E. F.; Wright, L. J.; Münck, E. *J. Am. Chem. Soc.* **1993**, *115*, 6746–6757.

(54) Keutel, H.; Kapplinger, I.; Jager, E. G.; Grodzicki, M.; Schunemann, V.; Trautwein, A. X. *Inorg. Chem.* **1999**, *38*, 2320–2327.

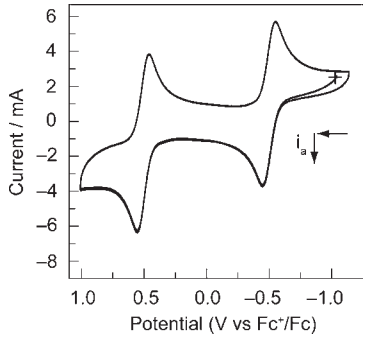

Figure 7. Cyclic voltammogram of **8a** in CH_2Cl_2 with 0.1 M $TBAPF_6$ as the supporting electrolyte. The reference potential is ferrocenium/ferrocene. The scan was initiated at the crosshair, and the potential was scanned anodically at a rate of 0.1 V s^{-1}.

(β, spin-down) delocalized on the corrole ring. Analysis of the gross orbital population and Mulliken spin density of +2.63 indicate an intermediate-spin d^5 configuration for the iron site, namely, $|(x^2-y^2)^2(xz)^\alpha(yz)^\alpha(z^2)^\alpha|$. The corrole ligand is one-electron oxidized and has an unpaired β-electron with a cumulated spin-density of −0.79; this β-electron occupies an extended molecular orbital with large contributions from the p_z atomic orbitals of the pyrrole N and of the meso C atoms (see Supporting Information, Table S4). This electronic structure is confirmed by TD-DFT calculations which yield an energy gap of ≈8000 cm^{-1} between the highest occupied d^β orbital (x^2-y^2) and the closely spaced {yz/xz} β-unoccupied orbital doublet; the highest occupied π^β corrole orbital is ∼7000 cm^{-1} below (x^2-y^2).

The predicted isomer shift δ_{calc} = 0.18 mm/s is in good agreement with the experimentally observed value δ_{exp} = 0.19 mm/s. The estimated EFG tensor is quasi-axial, η_{calc} = 0.05, with the large, positive component $eQV_{zz}/2$ = +3.28 mm/s oriented along the Fe−Cl vector and the smaller, negative components being roughly aligned with the NFeN medians (see Supporting Information, Table S3). Predicted isomer shifts have an uncertainty of 0.1 mm/s and quadrupole splitting of 0.5 mm/s.[55−58] Qualitative agreement is obtained for the calculated hyperfine coupling tensor A[59] (Supporting Information, Table S6). The A-tensor is the sum of the isotropic Fermi-contact term A^{FC}, the traceless spin-dipolar tensor A^{SD} and the orbital tensor A^L. The large energy gap between the occupied and unoccupied d^β orbitals suggests that the orbital component A^L to the hyperfine tensor is small and that the magnitude of the ZFS is mainly determined by the interaction of the ground orbital state with excited orbital states of different spin multiplicities. The calculated A^{SD} is nearly axial and collinear to the EFG tensor such that their largest, positive components are aligned. Along this direction, $A^{SD}{}_z$ overcomes the dominant (negative) contact contribution, A^{FC}, to yield an overall hyperfine coupling tensor A that has a small and positive component along the Fe−Cl vector and two large negative components parallel to the plane of the corrole ligand.

Table 3. Electrochemical Summary of Fe Corrole Complexes[a]

compound	E_1/V[b]	E_2/V[b]
7a[b]	0.46 V[c]	−0.91 V
8a	0.51 V	−0.51 V
8b	0.54 V	−0.56 V
8c	0.73 V	−0.26 V
FeCl Cor-Mes_3	0.54 V	−0.59 V
FeCl Cor-$(C_6F_5)_3$	0.88 V	−0.07 V
9a	0.53 V	−0.44 V

[a] Potential vs Fc^+/Fc in DCM and 0.1 M $TBAPF_6$. [b] E_2 is assigned to the reduction of the corrole cation, and E_1 is ascribed to metal reduction. [c] An additional redox event E_2' = 0.02 V falls between E_1 and E_2 that is consistent with a second metal based redox process in the dimer, see Supporting Information, Figure S4.

Our results agree well with published DFT,[20,26] and ab initio[59] studies of FeCl corrole complexes, which also are best described as intermediate-spin Fe(III) corrole radical cation systems.

Oxidation−Reduction Chemistry. Electrochemical investigations clearly show the influence of aryl meso-substitution on the reduction potentials of XC compounds. The cyclic voltammogram (CV) of **8a** that is shown in Figure 7 is typical of the iron corrole XC series and the A_3 corrole complexes; Table 3 lists the measured redox potentials for all complexes examined in this study. The initial scan begins anodically from a potential where [Fe(III)-corrole$^{+\bullet}$] is the electroactive species. On this basis, it is logical that the first wave (scanning anodically) corresponds to the corrole-based reduction potential and the second wave corresponds to the metal based reduction process. Two reversible redox events are observed. These results are in accordance with the electrochemistry of unmodified corroles for which the low-potential CV wave has been assigned to a Fe(III)/"Fe(IV)" couple and the high potential CV wave has been assigned to the corrole$^{+\bullet}$/corrole couple.[60] Whereas 4-*tert*-butylphenyl and mesityl meso-substituted corroles exhibit similar reduction potentials, the introduction of the strongly electron withdrawing pentafluorophenyl substituent shifts the potential range by 0.2−0.3 V to more positive potentials. The μ-oxo dimer **7a** shows three reversible CV waves (Supporting Information, Figure S4), which have been assigned to one corrole based oxidation at higher potentials and two Fe(III)/"Fe(IV)" processes at lower potential.[60] Alternatively, owing to the strong coupling of Fe centers across the oxo bridge, one metal based and two ligand based redox events is also plausible with the second metal based reduction shifted considerably anodic owing to strong coupling.

The redox chemistry of Hangman platforms may be manifested in the activation of small molecules by proton-coupled electron transfer (PCET).[1,2,61] The disproportionation of H_2O_2 to O_2 and H_2O is one important PCET process that is catalyzed by a wide variety of metalloproteins and enzymes.[62] As shown in Table 4 and shown in Supporting Information, Figure S21, the iron XC and HCX complexes catalyze this dismutation reaction. The time course of oxygen production (Supporting Information, Figure S21) is similar for each of the corroles: the reaction

(55) Neese, F. *Inorg. Chim. Acta* **2002**, *337*, 181–192.
(56) Godbout, N.; Havlin, R.; Salzmann, R.; Debrunner, P. G.; Oldfield, E. *J. Phys. Chem. A* **1998**, *102*, 2342–2350.
(57) Neese, F. *J. Phys. Chem.* **2003**, *118*, 3939–3948.
(58) Sinnecker, S.; Neese, F.; Noodleman, L.; Lubitz, W. *J. Am. Chem. Soc.* **2004**, *126*, 2613–2622.
(59) Roos, B. O.; Veryazov, V.; Conradie, J.; Taylor, P. R.; Ghosh, A. *J. Phys. Chem. B.* **2008**, *112*, 14099–14102.
(60) Simkhovich, L.; Mahammed, A.; Goldberg, I.; Gross, Z. *Chem.—Eur. J.* **2001**, *7*, 1041–1055.
(61) Rosenthal, J.; Chng, L. L.; Fried, S. D.; Nocera, D. G. *Chem. Commun* **2007**, 2642–2644.
(62) Nicholls, P.; Fita, I.; Loewen, P. C. *Adv. Inorg. Chem.* **2001**, *51*, 51–106.

Table 4. Catalytic Data for H_2O_2 Disproportionation of XC and HCX Iron Corroles and Related Porphyrin Analogues[a]

compound	TOF/min^{-1} [b]	TON (% conversion) [c]
FeCl(TMP)[d]	0.2	162
FeCl-Cor(C_6F_5)$_3$	79	173
FeCl-Cor(Mes)$_3$	15	95
FeCl-HPX-Mes[d]	102	533
8a	15	91
8b	21	96
8c	30	99
9a	16	70
FeCl-HPX-C_6F_5[d]	27	147

[a] In solutions of dichloromethane/methanol (3:1), for further details see the Supporting Information. [b] TOF recorded over initial 1 min reaction time. [c] After 60 min reaction time; significant decomposition of corrole over 60 min. [d] Data taken from ref 61, TMP = tetramesitylporphyrin, Mes = mesityl.

proceeds quickly during the initial stages of the reaction and over time the total amount of oxygen produced approaches an asymptotic limit. Oxygen cessation is likely a result of catalyst decomposition. Analysis of the reaction mixture by UV−vis and MS shows no sign of the formation of dimeric species **7** such as has been recently observed for water-soluble Fe corroles[63] or starting compound. Indeed, we cannot find any higher molar mass fragment and the color of the solution is completely bleached. We suspect the decomposition might go via an intermediate like **10**. As indicated by **10**, the meso positions of the corrole macrocycle are susceptible to attack by oxygen species; this type of decomposition pathway is prevalent for N4 macrocycles that access high oxidation states.[42−44]

The similar activities of **8a** to **9a** indicate that the hanging group has little effect of PCET reactivity. This result contrasts Hangman porphyrins and salens in which the carboxylic hanging group proved to be a prerequisite for high dismutation activity. We believe that the instability of the corrole may overwhelm the benefits of the Hangman effect on promoting dismutation activity, though this contention demands greater scrutiny.

Concluding Remarks

Hangman iron corroles are synthesized in good yields from a one-pot condensation of dipyrromethane with the aldehyde of a xanthene spacer followed by metal insertion using microwave irradiation. Mössbauer spectroscopy as well as DFT calculations of the iron corroles axially ligated by chloride are consistent with the description of a [Fe(III)Cl-corrole$^{+\bullet}$] in which the corrole ligand is redox non-innocent. The iron corrole complexes promote the catalytic dismutation of hydrogen peroxide. The peroxide dismutation reactivity reported here adds to the emerging theme that corroles are good at catalyzing two-electron activation of the O−O bond by dismutation in a variety of substrates including superoxide[64] and peroxynitrite.[65] The rate determining step in dismutation reactions is often the oxidation of peroxide by a metal-oxo center, two electrons above the initial state of the macrocycle complex.[6] In this case, the reaction is facilitated by the ease of reduction of a high valent state, and hence in principle a more oxidizing center should be more adept at dismutation. However, Gross and co-workers have recently shown that Fe corroles are potent dismutation catalysts beginning from the +3 oxidation state of the metal. The key intermediate in dismutation in Gross's system will therefore likely access either [Fe(IV)-corrole$^{+\bullet}$] or [Fe(V)-corrole], with the former more likely. Conversely, in the study here, **8** and **9** are one-electron oxidized above Gross' system. Hence, dismutation will access [Fe(V)-corrole$^{+\bullet}$]. While such an intermediate is expected to be more potent for dismutation, comparison of the far greater activity of Gross' system to that reported here suggests that formation of the higher oxidation state is more difficult to achieve, and a thermodynamic barrier is imposed on the dismutation. Moreover, the TON number in Gross' system is limited by Fe−O−Fe formation, but the corrole remains intact; thus, higher TON can be achieved by averting dimerization. In contrast, the systems reported here show degradation of the corrole framework. This result suggests that a more potent oxidizing intermediate such as [Fe(V)-corrole$^{+\bullet}$] is more susceptible to oxidative degradation of the macrocycle. This is commonly observed in porphyrin chemistry where the meso position is susceptible of oxidation.[66−68] These results taken together suggest that [M(III)-corrole], and not [M(III)-corrole$^{+\bullet}$] (or [M(IV) corrole]), is the proper precatalyst state needed for effective dismutation by corrole complexes.

Finally, the hanging group has been shown to be important for preorganizing the peroxide within the metal-oxo hanging cleft.[6] The same may be true here for the corroles, but the thermodynamic barriers and macrocycle instability for a [Fe(III)-corrole$^{+\bullet}$] precursor appear to subvert the benefits afforded by the hangman effect. These results suggest that the hangman effect will be more fully realized for [M(III)-corrole] systems.

Acknowledgment. M.S. thanks the German Academic Exchange Service (DAAD) for fellowship support within the Postdoc-Programme. The developments of new synthetic methods and synthesis of the new compounds were performed under the sole sponsorship of Eni S.p.A under the Eni-MIT Alliance Solar Frontiers Program, and characterization work was executed under the Division of Chemical Sciences, Geosciences, and Biosciences, Office of Basic Energy Sciences of the U.S. Department of Energy through Grant DE-FG02-05ER15745.[57]Fe Mössbauer spectra were recorded at Carnegie Mellon University, in Prof. Eckard Münck's laboratory; this research has been supported by the U.S. NIH (EB001475 to E.M.). S.A.S. wishes to thank Prof. Emile Bominaar for useful discussions. We thank Cassandra Cox and Andrew Horning for lifetime measurements. T.S. T. acknowledges the Fannie and John Hertz Foundation for a graduate research fellowship.

Supporting Information Available: Full experimental details for synthesis, NMR, MALDI-MS and high resolution ESI-MS of corrole compounds, crystallographic data, electronic spectra, CVs, computational details, and additional Mössbauer spectra. This material is available free of charge via the Internet at http://pubs.acs.org.

(63) Mahammed, A.; Gross, Z. *Chem. Commun.* **2010**, *46*, 7040–7042.
(64) Eckshtain, M.; Zilbermann, I.; Mahammed, A.; Saltsman, I.; Okun, Z.; Maimon, E.; Cohen, H.; Meyerstein, D.; Gross, Z. *Dalton Trans.* **2009**, 7879–7882.
(65) Mahammed, A.; Gross, Z. *Angew. Chem., Int. Ed.* **2006**, *45*, 6544–6547.
(66) Bhuyan, J.; Sarkar, S. *Chem.—Eur. J.* **2010**, *16*, 10649–10652.
(67) Balch, A. L.; Noll, B. C.; Zovinka, E. P. *J. Am. Chem. Soc.* **1992**, *114*, 3380–3385.
(68) Smith, K. M.; Brown, S. B.; Troxler, R. F.; Lai, J.-J. *Tetrahedron Lett.* **1980**, *21*, 2763–2766.